Phase Separation Behavior of (Palmitic Acid/Lignoceric Acid) Mixed Monolayer Based on a π–A Isotherm Measurement and a Scanning Probe Microscopic Observation

Miyuki Kuramori, Naoko Uchida, Kazuaki Suehiro, and Yushi Oishi*

Department of Applied Chemistry, Faculty of Science and Engineering, Saga University, 1 Honjo, Saga 840-8502

(Received October 21, 1999)

The aggregation state of a mixed monolayer of palmitic acid (C_{16}) and lignoceric acid (C_{24}) was investigated on the basis of a π–A isotherm measurement and a scanning probe microscopic observation. The independence of the plateau and collapse pressures on the monolayer composition and the additivity of the average molecular area exhibited that the C_{16} and C_{24} molecules were immiscible in the monolayer, indirectly suggesting the presence of phase-separated domains in the system. Two kinds of regions with different heights were apparently observed on an atomic force microscope image of the mixed monolayers. The change in the area fraction with the composition, the film thickness and the difference in the lateral force of the two regions revealed that the (C_{16}/C_{24}) mixed monolayer was in a phase-separated state. This phase separation is probably due to an enthalpic contribution based on the difference in cohesive energy of each alkyl chain.

The increased attention on phase-separated mixed monolayers originates from potential applications as molecular templates for protein crystallization[1] and adsorption,[2] patterning layers in molecular photodiode[3] and selective layers in biosensors.[4] These functions depend on the size, distribution and density of phase-separated domains in mixed monolayers. Therefore, a systematic understanding on the phase separation mechanism in a mixed monolayer appears to be an essential step in the design and construction of functionalized structures in a two-dimensional system.

The miscibility and molecular interaction for mixed monolayers of various amphiphilic molecules have been examined by π–A isotherm analyses based on the additive rule with respect to the molecular area,[5—12] mechanical properties,[13—16] evaporation behavior,[17,18] equilibrium spreading pressure,[19] and vapor pressure.[20] However, it has turned out to be difficult to distinguish the complete miscibility from phase separation on the basis of a macroscopic π–A isotherm measurement. Thus, direct microscopic observations are useful in the determination of whether the components are miscible or phase separate, and also in characterization of the phase-separated domain in the mixed monolayer.

Recently, electron,[1,21] fluoresence,[22—30] Brewster angle,[31] phase contrast,[32] surface plasmon,[4] and scanning probe[2,3,33—39] microscopies have been allowed to characterize the surface morphology of a mixed monolayer. Of these methods, a scanning probe microscope may be most useful because the vertical and lateral resolutions of angstrom order are enable to detect the height difference and domain size on the nanometer scale at a monolayer surface. Also, a lateral force measurement by the microscope allows to identify the chemical species and to clarify the difference in the aggregation state in a mixed monolayer. However, because most of these studies use limited samples, or are devoted to the development of analytical methods and the evaluation of mechanical properties of thin films, little has been done concerning a systematic understanding of phase separation mechanism in a monolayer. The phase separation in a monolayer depends on many factors involving electrostatic interaction, molecular chirality and so on besides thermodynamic parameters such as the subphase temperature and surface pressure. Hence, to obtain a general concept of phase separation in a monolayer, it is necessary to investigate a simple experimental system as a first step. A fatty acid monolayer is probably suitable for the experimental system, because the aggregation state of the monolayer on a pure water surface depends on only two factors: the thermal molecular motion and the cohesive force among hydrophobic portions.

In this study, the aggregation state of a mixed monolayer of fatty acids with different alkyl chain lengths was investigated on the basis of a π–A isotherm measurement and a scanning probe microscopic observation. We used palmitic and lignoceric acids as binary components because specific interaction, except for a cohesive force among alkyl chains, does not act between these acids, and also that each component is easily detected owing to a large difference (eight methylene units) in the molecular length when the components are phase separate in the mixed monolayer.

Experimental

Surface Pressure–Area (π–A) Isotherm Measurement.

Palmitic ($CH_3(CH_2)_{14}COOH$, C_{16}) and lignoceric ($CH_3(CH_2)_{22}COOH$, C_{24}) acids with a purity >99.99% were used as monolayer components. Benzene of spectroscopic quality was used as a spreading solvent. Benzene solutions

of C_{16}, C_{24}, and (C_{16}/C_{24}) mixtures with molar fractions of 80/20, 60/40, 50/50, 40/60, and 20/80 were prepared at concentrations of 2.0×10^{-3}, 8.0×10^{-4} and 8.0×10^{-4} mol L^{-1}, respectively. The subphase water was purified by a Ultra High Quality Polishing System (Elgastat Co., Ltd.). The sample solution was spread on a water surface at a subphase temperature, T_{sp}, of 293 K. The dimensions of the trough were 560 mm in length, 150 mm in width and 5 mm in depth. T_{sp} was adjusted to 293 ± 0.5 K by circulating constant-temperature water around the aluminum support of the trough. Also, the room temperature was adjusted to the same temperature as T_{sp} by using an air-conditioner. A surface pressure–area (π–A) isotherm of each monolayer was measured under compression by two barriers at an area change rate of 8.6×10^{-4} nm^2 $molecule^{-1}$ s^{-1} with a microprocessor-controlled film balance system (FSD-300, USI System Co., Ltd.).

Scanning Probe Microscopic Observation. Each monolayer was compressed to a surface pressure of 20.0 ± 0.5 mN m^{-1} at the same area change rate as a π–A isotherm measurement. The monolayer was transferred onto freshly cleaved mica (Okabe Mica) by the horizontal drawing-up method[40] at a transfer rate of 1 mm min^{-1}. The transfer ratio for each monolayer was unity, indicating that the mica substrate was completely covered by each monolayer. Atomic force microscope (AFM) and lateral force microscope (LFM) images of the monolayer were obtained with an SPA 300 unit together with an SPI 3700 control station (Seiko Instruments Industry, Co., Japan) in air at 293 K. A 20 μm×20 μm scan head and a silicon nitride tip of pyramidal shape on a triangular cantilever with a spring constant of 0.02 N m^{-1} were used. Images were recorded at a scan rate of 2 Hz in the "constant-force" mode; that is, feedback electronics and the corresponding software were used to keep the cantilever at constant deflection and to measure the sample motion. The applied force during scanning was 8—10 nN in an attractive force range. Calibrations of the scanner were performed with a 3 μm-pitched sample (VLSI, Stand. Inc.) for a lateral displacement and with steps on cadmium arachidate film[41] for a vertical displacement. The monolayer thickness was evaluated from the hole depth for an AFM image with a scan area of 1 μm×1 μm at the minimal force very closely where the probe was pulled off the sample surface, after artificially piercing a hole with an area of 100 nm×100 nm through the monolayer with the AFM probe at an applied force of 5 nN in a repulsive force range. In order to obtain the maximum LFM signal, the sample surface was scanned along the direction perpendicular to the cantilever long axis.

Results and Discussion

π–A Isotherm Behavior of the Mixed Monolayer. Figure 1 shows the π–A isotherms of pure C_{16}, C_{24}, and of (C_{16}/C_{24}) mixed monolayers with different molar fractions on the water surface at a T_{sp} of 293 K. This figure was illustrated by sliding the abscissae corresponding to the seven molar fractions for clarity. Some microscopic studies[32,42—44] have revealed that the pure C_{16} and C_{24} molecules form isolated two-dimensional domains immediately after spreading a solution and these domains aggregate together to be a morphologically homogeneous state during compression at a T_{sp} of 293 K and at a neutral pH range. The π–A isotherm of the pure palmitic acid monolayer (C_{16}/C_{24}: 100/0) exhibited a sharp rise in surface pressure at a surface area of ca. 0.25 nm^2 $molecule^{-1}$. This increase in surface pressure results from contact between two-dimensional crystalline domains grown just after spreading a solution by surface compression. For a pure lignoceric acid monolayer (C_{16}/C_{24}: 0/100), a plateau region was observed in an area range of 0.21—0.23 nm^2 $molecule^{-1}$ on the π–A isotherm. The plateau region appears owing to the consumption of compression energy for the crystal transition from a hexagonal system to a rectangular one.

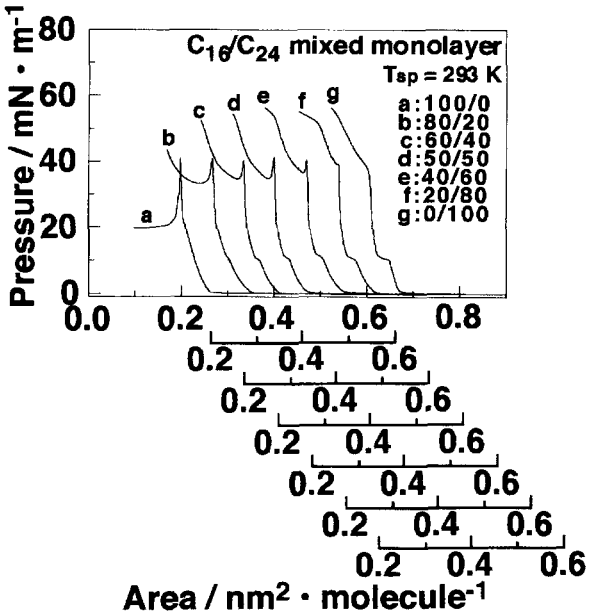

Fig. 1. π–A Isotherms of pure C_{16}, C_{24}, and of (C_{16}/C_{24}) mixed monolayers with molar fractions of 80/20, 60/40, 50/50, 40/60, and 20/80 on the water surface at T_{sp} of 293 K.

The characteristic π–A isotherm behavior was observed for the (C_{16}/C_{24}) mixed monolayers. Every isotherm exhibited a plateau region at a surface pressure of ca. 10 mN m^{-1}, which was the same as the plateau pressure of the pure C_{24} monolayer. The plateau pressure corresponds to the compression energy required for the crystal transition from a hexagonal system to a rectangular one. Hence, it seems that the aggregated regions of C_{24} molecules exist in the mixed monolayers. Furthermore, the area range of the plateau region decreased with a decrease in the C_{24} content. This suggests a decrease in the C_{24} aggregated region in the mixed monolayers. Additional information about the miscibility of C_{16} and C_{24} in the monolayer is obtained from the collapse pressure behavior.[14,15,45,46] According to the thermodynamic phase rule, the variation of the collapse pressure with the molar fraction of the components appears to be an indication of miscibility, while the constancy of the collapse pressure reveals segregation. Two collapse pressures of ca. 40 and

55 mN m^{-1} remained almost constant for all compositions, and were identical to the collapse pressure of the pure C_{16} and C_{24} monolayers, respectively. Of the two components, C_{16}, which forms a relatively less stable monolayer, probably squeezes out first, followed by a further compression of the C_{24} component. The π–A isotherm behavior around the plateau region and the collapse point suggests the phase separation of the (C_{16}/C_{24}) mixed monolayer.

The miscibility behavior of the components in the mixed monolayers may be examined by the change in the average molecular occupied area as a function of the composition. The following additivity rule is valid for a mixed system with ideal mixing or complete immiscibility of components:[7—12,47]

$$A_{12} = N_1A_1 + N_2A_2,$$

where A_{12} is the average molecular area in a composite film, N_1 and N_2 are the molar fractions of the components, and A_1 and A_2 are the molecular area in the two single component films at the same surface pressure. A deviation from the additivity rule leads to the conclusion that the components of the system are miscible. The measured molecular areas for the (C_{16}/C_{24}) mixed monolayers are plotted against the monolayer composition at constant surface pressures of 5, 10, 15, and 20 mN m^{-1} in Fig. 2. The dotted line illustrates the additive relationship. The average molecular area values measured in all compositions for all surface pressures match the calculated values in a margin of statistical error, indicating that the components are ideal mixing or complete immiscible being irrespective of the surface pressure. Putting the above-mentioned results together, it is reasonable to consider that the C_{16} and C_{24} molecules are phase separate in the mixed monolayers.

Surface Morphology of Single Component Monolayers. Figures 3(a) and 3(b) show AFM images of the palmitic acid (C_{16}/C_{24}: 100/0) and the lignoceric acid (C_{16}/C_{24}: 0/100) monolayers with a scan area of 5 μm×5 μm, respectively. The surface morphology of the C_{16} and C_{24} monolayers was very smooth with an average surface roughness, R_a,[48] of 0.1—0.2 nm, excepting holes. The holes correspond to the dark area of the images, with the brighter being the surface of the films. In the 5 μm×5 μm scan, there are ca. 0.6 holes μm^{-2} (or ca. 15 holes in the entire scan) with a lateral size of 20—150 nm. Such a surface morphology containing holes has been often observed for the fatty acid salt monolayer.[41,49,50] The C_{16} and C_{24} monolayers are the crystalline monolayer in which the crystalline domains grown immediately after spreading a solution are gathered together to form an apparently homogeneous monolayer by surface compression. During the compression process, some vacancies among the crystalline domains remain due to compression at a relatively high speed. Hence, the observed holes in the monolayers probably correspond to vacancies which remain due to structural fixation induced by compression. The film thickness of the C_{16} and C_{24} monolayers were evaluated to be 1.3 ± 0.1 nm and 2.9 ± 0.1 nm, respectively, by piercing a hole through the monolayer. The thickness of the C_{16} monolayer was smaller than the calculated molecular length (1.9 nm, distance between carbons of terminal methyl and carboxyl group) of C_{16} of the extended CPK molecular model, although that of the C_{24} monolayer was comparable to the calculated molecular length (2.9 nm) of C_{24}. It has been reported that the measured thickness of fatty acid monolayers by AFM is often less than the molecular length owing to an AFM probe indentation into a monolayer, depending on the mechanical response of the monolayer.[37,41,51—54] The degree of molecular aggregation of the C_{16} monolayer is very low because of the shorter alkyl chain, which causes a deeper indentation of the AFM probe into the monolayer. Hence, the low degree of molecular aggregation for the C_{16} monolayer was probably reflected in the smaller measured value of the film thickness. Another reason for the discrepancy in the monolayer thickness may be sought in the conformation of the alkyl chain. The weak cohesive force, in other words, the active thermal molecular motion of the C_{16} molecule in the monolayer leads to the introduction of many gauche conformation units into the alkyl chain of the C_{16} molecule. Consequently, the C_{16} monolayer thickness truly becomes smaller compared with the calculated molecular length based on the CPK model (all-*trans* conformation).

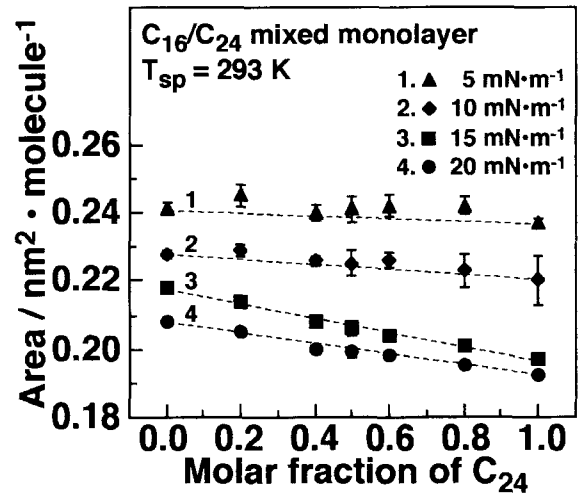

Fig. 2. Composition dependence of molecular occupied area at constant surface pressures of 5, 10, 15, and 20 mN m^{-1}. Error bar represents a 95% statistical error for nine π–A isotherms.

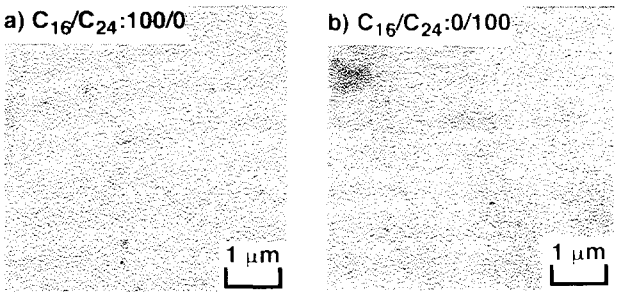

Fig. 3. AFM images of single component monolayers of the C_{16} (a) and C_{24} (b) transferred at a surface pressure of 20 mN m^{-1} on the water surface at T_{sp} of 293 K.

In any case, the surface flatness of the C_{16} and C_{24} monolayers and the distinct difference in their film thickness (ca. 1.6 nm) should be useful in a determination using a scanning probe microscope of whether the C_{16} and C_{24} molecules are miscible or immiscible in the mixed monolayer, as shown later.

Molecular Aggregation State of Mixed Monolayers. Figure 4 shows AFM images of the (C_{16}/C_{24}: 80/20, 60/40,

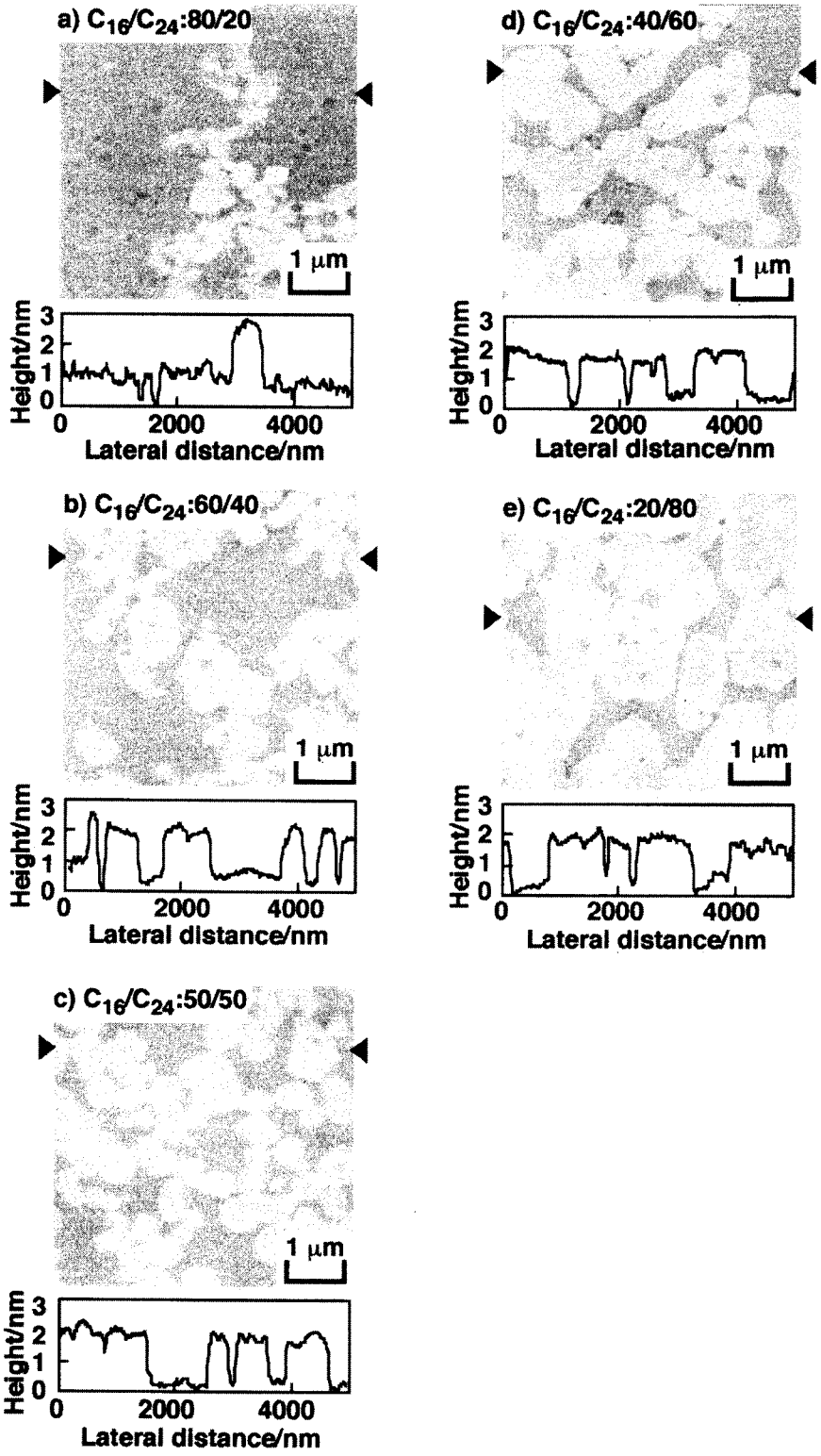

Fig. 4. AFM images of the (C_{16}/C_{24}) mixed monolayers with molar fractions of (a) 80/20, (b) 60/40, (c) 50/50, (d) 40/60, and (e) 20/80 on the water surface at T_{sp} of 293 K, as well as topographical contour plot along the line connected by triangular at both sides in AFM images.

50/50, 40/60, and 20/80) mixed monolayers with a scan area of 5 μm×5 μm, as well as topographical contour plots along the supposed line which was connected by triangular markers at both sides of each AFM image. The brighter and darker portions correspond to the higher and lower regions of the monolayer surface, respectively. The higher flat-topped domains and the lower surrounding matrix were observed at all AFM images. Apparently, the area of brighter portion corresponding to the domain region increased consistently with the C_{24} content. Then, the area fraction of the higher (brighter) region was plotted against the molar fraction of C_{24} in a sample solution in Fig. 5. The dotted line illustrated the proportional relationship of one to one. The area fraction of the higher (domain) regions was in good agreement with the molar fraction of C_{24}. This indicates a complete segregation of C_{24} molecules from C_{16} molecules in the mixed monolayer. The thickness of the higher and lower regions in every mixed monolayer agreed with that of the pure C_{24} and C_{16} monolayers, respectively, as shown in Fig. 6.[55] It is, therefore, apparent that the domains and the surrounding matrix are composed of the C_{16} and C_{24} molecules, respectively. In addition, the domains tend to aggregate together, rather than isolate even at a (C_{16}/C_{24}) molar fraction of 80/20 (Fig. 4a). The isolation of domains in a matrix causes thermodynamic instability by the free energy difference of the C_{16} and C_{24} molecules due to their cohesive energy difference. Hence, it seems that the interfacial region between the domain and matrix may decrease; that is, domains aggregate together to reduce the free energy difference. This is reflected in the formation of larger domains by an increase in the C_{24} content, which leads to a conversion of the aggregated regions of C_{24} to a matrix at a molar fraction of 20/80.

Figure 7 shows a LFM image of the (C_{16}/C_{24}: 50/50) mixed monolayer (a), the lateral force (friction) loop (b) and the corresponding topographical contour plot in the AFM

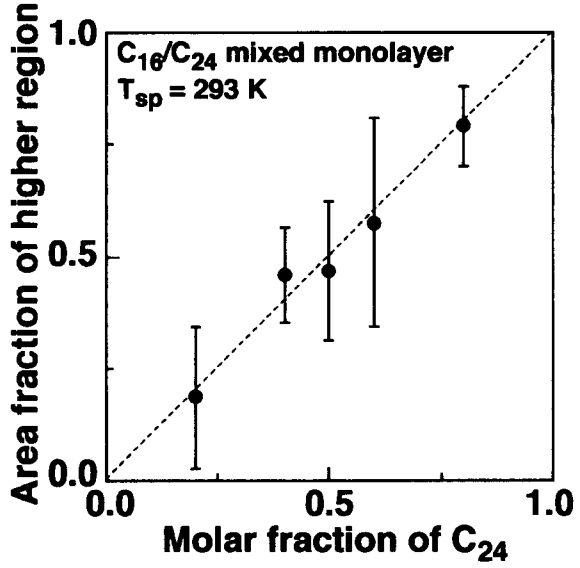

Fig. 5. Composition dependence of area fraction of higher region in AFM images. Error bar represents a 95% statistical error at ten different scan regions.

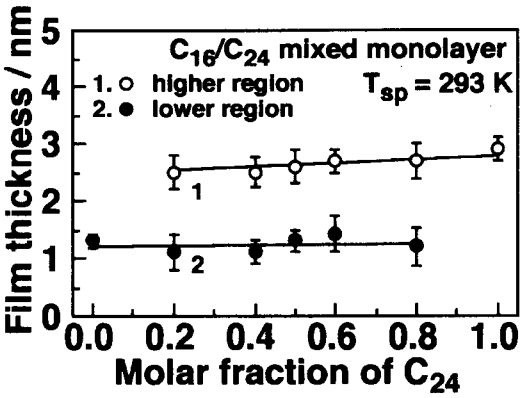

Fig. 6. Composition dependence of monolayer thickness. Error bar represents a 95% statistical error of fifty different positions in ten scan regions.

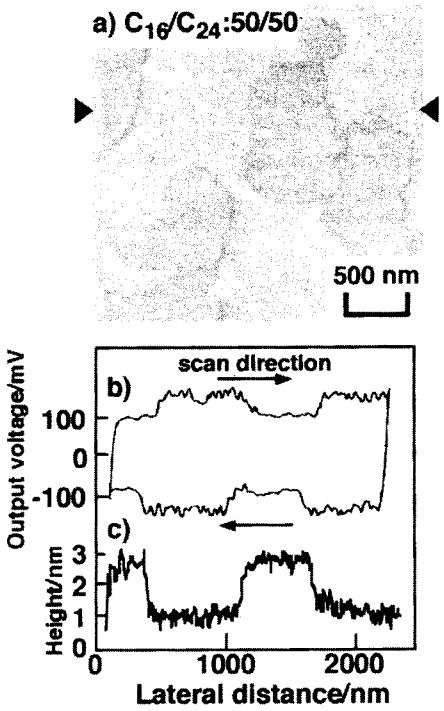

Fig. 7. LFM image of the (C_{16}/C_{24}: 50/50) mixed monolayer (a), the lateral force loop along the line connected by triangular marks at the LFM image (b) and the corresponding topographical contour plot (c). The offset in horizontal direction arises from piezoelectric hysterisis.

image, which was simultaneously recorded with the LFM image (c). The lateral force loop was obtained by forward and reverse scans along the supposed line, which was connected by triangular marks at both sides in the LFM image. The contrast in the LFM image corresponds to the magnitude of the output voltage from the photodiode, which is proportional to the magnitude of the lateral force. The brighter part in Fig. 7(a) corresponds to the region with a higher lateral force, and the darker part to that with a lower one. Figure 7(a) clearly exhibits two kinds of regions in the lateral force. Figure 7(b) obviously shows a reversal of magnitude of the lateral force depending on the scanning direction, indicating

that the difference in lateral force is not due to a change in the topography. That is, the magnitude of the lateral force contains a friction force and/or adhesive force contributions. A comparison of Figs. 7(b) and 7(c) reveals that the lateral force change synchronizes with the topographical one, and also that larger and smaller lateral forces correspond to lower and higher positions in the topography. This implies an opposite contrast of LFM and AFM images. Accordingly, the domains of C_{24} and the surrounding flat matrix of C_{16} correspond to those regions with a lower lateral force and a higher one, respectively. As described in Fig. 3, the degree of molecular aggregation of the C_{16} molecules is lower than that of the C_{24} molecules because of the shorter alkyl chain. Thus, the probe easily penetrates in the monolayer, resulting in an increase in the contact area between the probe and the monolayer sample. This larger contact area should cause a higher dynamic friction force in the C_{16} matrix.

In general, the miscibility in mixed monolayers is determined by the steric compatibility of amphiphilic molecules and their intermolecular interactions at a given temperature. The skelton structure of the C_{16} molecule is the same as that of C_{24}, indicating steric compatibility of the components. That is, the components tend to miscible in the mixed monolayer. However, scanning probe microscopic observations (Figs. 4, 5, 6, and 7) proved phase separation of the components. The subphase was in the neutral pH range in this study, which corresponds to an unionized state of the carboxylic group of both fatty acids.[56] Hence, the immiscibility of the C_{16} and C_{24} molecules is dominated by interactions in the hydrophobic region of the monolayers. The difference in the cohesive energy between the C_{16} and C_{24} molecules is ca. 55 kJ mol^{-1} (7 kJ mol^{-1} per methylene unit).[57] It is, therefore, reasonable to consider that the cohesive energy difference of ca. 55 kJ mol^{-1} reduces the interaction potential overcoming the entropic contribution, which results in a phase separation of the (C_{16}/C_{24}) mixed monolayers.

Conclusion. The fatty acids of C_{16} and C_{24} are phase separated in the mixed monolayer at a T_{sp} of 293 K. The present study suggests that the difference in the cohesive energy of the components affects the immiscibility in the mixed monolayers. Whether amphiphilic molecules are miscible or immiscible in the monolayer and the phase-separated structure may depend on various factors, such as the intermolecular interaction, particularly an electrostatic one, and the subphase temperature. A further systematic investigation is required to elucidate the phase separation mechanism of the multicomponent monolayer.

The authors thank Dr. Masao Suzuki (NOF Co.) for providing the samples of palmitic and lignoceric acids used in this study. This research was supported in part by a Grant-in-Aid for Scientific Research (B), No. 09450039 from the Ministry of Education, Science, Sports and Culture.

References

1 R. H. Newman and P. S. Freemont, *Thin Solid Films*, **18**, 284 (1996).
2 A. Takahara, K. Kojio, S. Ge, and T. Kajiyama, *J. Vac. Sci. Technol. A*, **14**, 1747 (1996).
3 M. Fujihira, M. Sakomura, D. Aoki, and A. Koike, *Thin Solid Films*, **168**, 273 (1996).
4 B. Fisher, S. P. Heyn, M. Egger, and H. E. Gaub, *Langmuir*, **9**, 136 (1993).
5 W. D. Harkins and R. T. Florence, *J. Chem. Phys.*, **6**, 847 (1938).
6 T. Isemura and K. Hamaguchi, *Mem. Inst. Sci. Ind. Res. Osaka Univ.*, **8**, 131 (1951).
7 L. de Bernard, *Bull. Soc. Chim. Biol.*, **40**, 161 (1958).
8 R. A. Demel, L. L. M. Van Deenen, and B. A. Pethica, *Biochim. Biophys. Acta*, **135**, 11 (1967).
9 D. A. Cadenhead and R. J. Demchak, *J. Colloid Interface Sci.*, **30**, 76 (1969).
10 I. S. Costin and G. T. Barnes, *J. Colloid Interface Sci.*, **51**, 106 (1975).
11 K. Motomura, T. Terazono, H. Matuo, and R. Matuura, *J. Colloid Interface Sci.*, **57**, 52 (1976).
12 K. J. Bacon and G. T. Barnes, *J. Colloid Interface Sci.*, **67**, 70 (1978).
13 G. E. Boyd and F. Vaslow, *J. Colloid Sci.*, **13**, 275 (1958).
14 M. Nakagaki and N. Funasaki, *Bull. Chem. Soc. Jpn.*, **47**, 2482 (1974).
15 T. Handa and M. Nakagaki, *Colloid Polym. Sci.*, **257**, 374 (1979).
16 O. Albrecht, H. Gruler, and E. Sackmann, *J. Colloid Interface Sci.*, **79**, 319 (1981).
17 V. K. LaMer, L. A. G. Aylmore, and T. W. Healy, *J. Phys. Chem.*, **67**, 2793 (1963).
18 I. S. Costin and G. T. Barnes, *J. Colloid Interface Sci.*, **51**, 122 (1975).
19 A. Angelova, J. De Coninck, and R. Ionov, *Supramol. Sci.*, **4**, 207 (1997).
20 R. E. Pagano and N. L. Gershfeld, *J. Phys. Chem.*, **76**, 1238 (1972).
21 A. Fischer and E. Sackmann, *J. Colloid Interface Sci.*, **112**, 1 (1986).
22 W. M. Heckl, D. A. Cadenhead, and H. Möhwald, *Langmuir*, **4**, 1352 (1988).
23 C. L. Hirshfeld and M. Seul, *J. Phys.*, **51**, 1537 (1990).
24 K. M. Maloney and D. W. Grainger, *Chem. Phys. Lipids*, **65**, 31 (1993).
25 K. Y. C. Lee, J. F. Klinger, and H. M. McConnell, *Science*, **263**, 655 (1994).
26 J. Slotte, *Biochim. Biophys. Acta*, **1235**, 419 (1995).
27 H. M. McConnell, *Proc. Natl. Acad. Sci. U.S.A.*, **93**, 15001 (1996).
28 S. Perkovic and H. M. McConnell, *J. Phys. Chem.*, **101**, 381 (1997).
29 L. D. Worthman, K. Nag, P. J. Davis, and K. M. W. Keough, *Biophys. J.*, **72**, 2569 (1997).
30 K. Tanaka, P. A. Manning, V. K. Lau, and H. Yu, *Langmuir*, **15**, 600 (1999).
31 A. Angelova, M. Van der Auweraer, R. Ionov, D. Vollhardt, and F. C. De Schryver, *Langmuir*, **11**, 3167 (1995).
32 H. Hosoi, H. Akiyama, E. Hatta, T. Ishii, and K. Mukasa, *Jpn. J. Appl. Phys.*, **36**, 6927 (1997).
33 R. M. Overney, E. Meyer, J. Frommer, D. Brodbeck, R. Lüthi, L. Howald, H. J. Güntherodt, M. Fujihira, H. Takano, and Y. Gotoh, *Nature*, **359**, 133 (1992).

34 R. M. Overney, E. Meyer, J. Frommer, H. J. Güntherodt, M. Fujihira, H. Takano, and Y. Gotoh, *Langmuir*, **10**, 1281 (1994).

35 J. M. Solletti, M. Botreau, F. Sommer, T. M. Duc, and M. R. Celio, *J. Vac. Sci. Technol. B*, **14**, 1492 (1996).

36 S. Jacobi, L. F. Chi, and H. Fuchs, *J. Vac. Sci. Technol. B*, **14**, 1503 (1996).

37 D. D. Koleske, W. R. Barger, G. U. Lee, and R. J. Colton, *Mat. Res. Soc. Symp. Proc.*, **464**, 377 (1997).

38 K. Iimura and T. Kato, *Colloid. Surf.*, **143**, 491 (1998).

39 K. Suga, Y. Iwamoto, H. Shibata, N. Yamada, and M. Fujihira, *Thin Solid Films*, **327—329**, 837 (1998).

40 Y. Oishi, T. Kuri, Y. Takashima, and T. Kajiyama, *Chem. Lett.*, **1994**, 1445.

41 A. Schaper, L. Wolthaus, D. Möbius, and T. M. Jovin, *Langmuir*, **9**, 2178 (1993).

42 N. Uyeda, T. Takenaka, K. Aoyama, M. Matsumoto, and Y. Fujiyoshi, *Nature*, **327**, 319 (1987).

43 T. Takoshima, A. Matsuda, and K. Mukasa, *Thin Solid Films*, **51**, 210 (1992).

44 Y. Oishi, H. Kozuru, K. Shuto, and T. Kajiyama, *Trans. Met. Res. Soc. Jpn.*, **15A**, 563 (1994).

45 G. L. Gaines, Jr., "Insoluble Monolayers at Liquid-Gas Interface," Interscience, New York (1966).

46 G. Gabrielli and P. Baglioni, *J. Colloid Interface Sci.*, **83**, 221 (1981).

47 G. L. Gaines, Jr., *J. Colloid Interface Sci.*, **21**, 315 (1966).

48 The average surface roughness, R_a was designated by the equation $R_a = (1/L)\int_0^\infty |H(x)|dx$, where L and $H(x)$ are the lateral distance of 5 μm (in this study) and the height profile along the lateral direction, respectively.

49 H. G. Hansma, S. A. C. Gould, P. K. Hansma, H. E. Gaub, M. L. Longo, and J. A. N. Zasadzinski, *Langmuir*, **7**, 1051 (1991).

50 R. Viswanathan, D. K. Schwartz, J. Garnaes, and J. A. N. Zasadzinski, *Langmuir*, **8**, 1603 (1992).

51 L. F. Chi, M. Anders, H. Fuchs, R. R. Johnston, and H. Ringsdorf, *Science*, **259**, 213 (1993).

52 Y. F. Dufrêne, W. R. Barger, J. D. Green, and G. U. Lee, *Langmuir*, **13**, 4779 (1997).

53 M. Hartig, L. F. Chi, X. D. Liu, and H. Fuchs, *Thin Solid Films*, **262**, 327 (1998).

54 T. Umeda, M. Kuramori, K. Suehiro, and Y. Oishi, *Rept. Prog. Polym. Phys. Jpn.*, **42**, 323 (1999).

55 Although the higher region slightly increased with an increase in C_{24} content, the increment is not a significant one because it exists in a margine of statistical error.

56 Y. Oishi, Y. Takashima, K. Suehiro, and T. Kajiyama, *Langmuir*, **13**, 2527 (1997).

57 J. N. Israelachvili, "Intermolecular and Surface Forces," Academic Press, London (1985).